DANISH METEOROLOGICAL INSTITUTE

——— SCIENTIFIC REPORT ———

02-05

The structure and dynamics of the atmospheric boundary layer

Niels Woetmann Nielsen

COPENHAGEN 2002

ISSN Nr. 0905-3263 (printed)
ISSN Nr. 1399-1949 (online)
ISBN-Nr. 87-7478-456-0

The structure and dynamics of the atmospheric boundary layer

Niels Woetmann Nielsen
Danish Meteorological Institute, Copenhagen, Denmark

May 31, 2002

1. Introduction

The goal of this lecture note is to give the reader a physical understanding of the basic physics determining the evolution with time of the unsaturated atmospheric boundary layer (ABL). The ABL is usually in a turbulent state, basically as a result of dynamical and thermodynamical instability. The former instability is related (but not uniqly) to the socalled "no slip" condition at the surface, which means that molecular friction forces the wind speed to zero at the surface.

The lecture note will not cover interesting, but rather complex topics like the cloudy ABL, the horizontally inhomogeneous ABL, similarity theory for the ABL and its surface layer, baroclinicity in the ABL, spectral aspects of turbulence, and higher order moment equations governing the turbulent flow with the turbulent kinetic energy equation as an exception.

2. The Ekman spiral

The ABL is the bottom layer of the troposphere. It is of highly practical interest because almost all human activity takes place in this layer. From a physical point of view it is also meaningfull to speak about the ABL. In contrast to the free atmosphere, which is the troposphere above the ABL, friction becomes a significant force in the ABL. One immediate consequence is that the wind becomes highly ageostrophic even for a flow without curvature. In the Northern Hemisphere (NH) the wind turns clockwise with height in the ABL, giving rise to the "Ekman spiral". This name has been given in honour of its inventor Ekman, 1905, and because the arrowhead of the wind vector when drawn as function of height above the surface describes a spiral around the arrowhead of the geostrophic wind vector. The latter is here considered to be constant with height, i.e. the ABL is assumed to be barotropic. Complexity is added if the ABL is baroclinic and consequently with a geostrophic wind varying with height. An "ideal" Ekman spiral in the barotropic ABL is shown in Figure 1. The spiral is formed by the force balance between the horizontal pressure gradient force, the (turbulent) friction force and the Coriolis force. The former is constant with height (in a barotroic ABL), while the frictional force and the Coriolis force decreases and increases with height, respectively. If the flow in the ABL has curvature the centripetal force must be added to the list of forces.

The force balance is illustrated in Figure 2. Note that the friction force is *not* in general in the opposite direction of the wind, as shown in many text books. At the top of the ABL the friction force becomes negligible, and in case of no curvature the force balance is then reduced to the geostrophic balance.

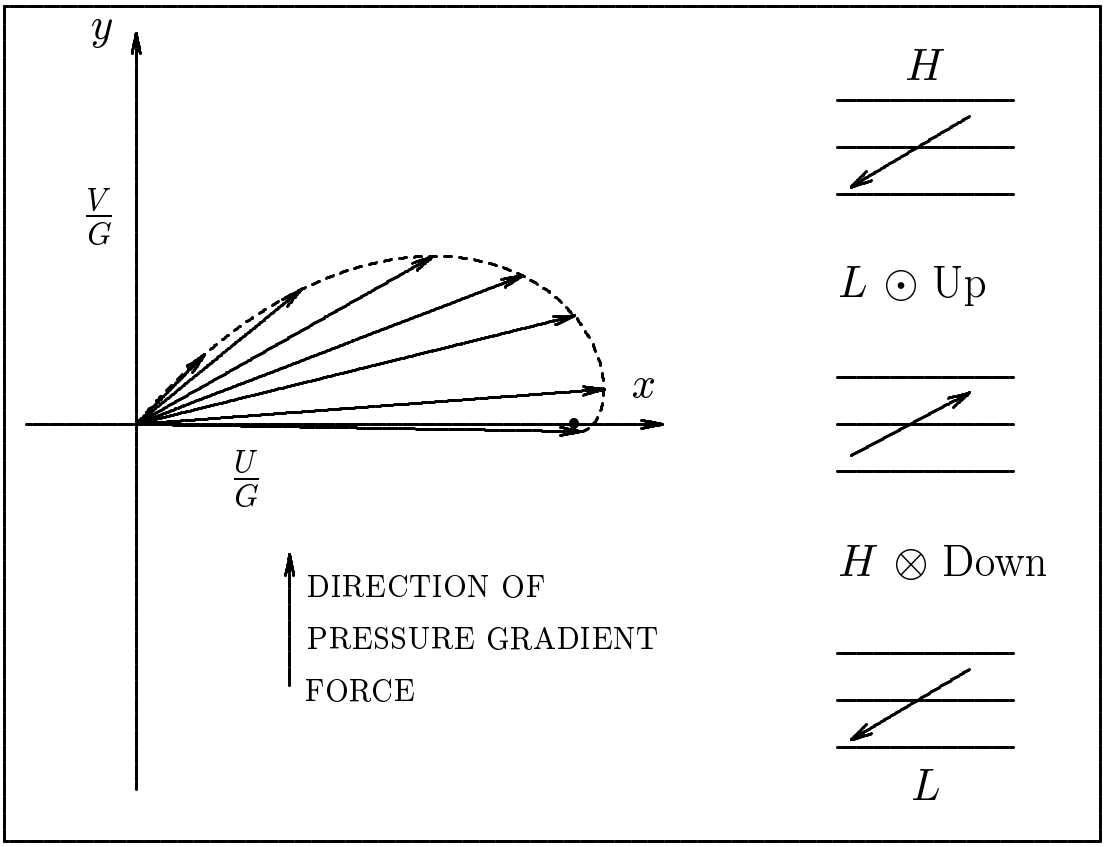

Figure 1: Idealized Ekman spiral, showing the turning of the wind with height in a Northern Hemispheric ABL. The coordinate system has its x-axis in the direction of the geostrophic wind $\vec{V}_g$ ($|\vec{V}_g| = G$). The cross isobar flow induces rising motion in the ABL in low pressure areas (L) and sinking motion in high pressure areas (H), as indicated in the right part of the figure.

3. Turbulence

Turbulence is the most fascinating feature of the flow in the ABL. It can also occur occasionally in connection with jet streams in the free atmosphere (clear air turbulence). Turbulence is nearly always present in the ABL, in particular in its bottom part. It is therefore a relevant question to ask: What is turbulence? The question is easy to ask, but it is very difficult to give a thorough answer. In this lecture note the goal is to illustrate the physical meaning of turbulence. In a way turbulence comes out of a specific mathematical treatment of the equations governing the atmosphere. The principle is shown by considering for example the x-component of the momentum equation (per unit mass). This equation reads

$$\frac{\partial U}{\partial t} + U\frac{\partial U}{\partial x} + V\frac{\partial U}{\partial y} + W\frac{\partial U}{\partial z} = \Sigma F_{xi}. \tag{1}$$

Here U is the velocity component in the x-direction and V and W are the velocity components in the y- and z-direction, respectively. The sum on the right hand side (rhs) symbolizes the forces acting in the x-direction. On the left hand side (lhs) the first term is the rate of change with time of U at a given point and

$$ADV = U\frac{\partial U}{\partial x} + V\frac{\partial U}{\partial y} + W\frac{\partial U}{\partial z} \tag{2}$$

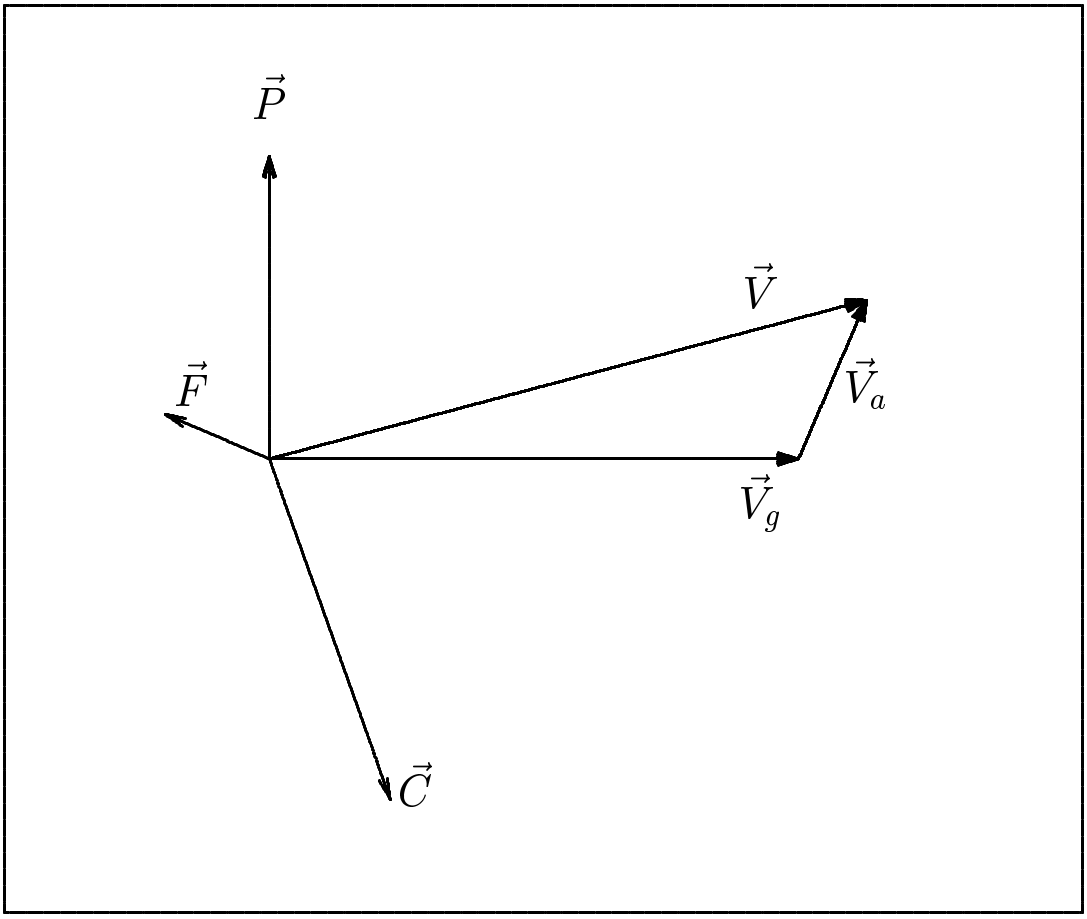

Figure 2: Balance of the turbulent frictional force ($\vec{F}$), the horizontal pressure gradient force ($\vec{P}$) and the Coriolis force ($\vec{C}$) in the upper part of the ABL. The wind velocity ($\vec{V}$) is the sum of the geostrophic wind ($\vec{V}_g$) and the ageostrophic wind ($\vec{V}_a$). Note that $\vec{V}_a$ is perpendicular to $\vec{F}$.

is the advection of U-momentum by the 3-dimensional wind $\vec{V} = (U, V.W)$. Using mathematical manipulation we can rewrite ADV as

$$ADV = \frac{\partial U^2}{\partial x} + \frac{\partial UV}{\partial y} + \frac{\partial UW}{\partial z} - U \cdot (\frac{\partial U}{\partial x} + \frac{\partial V}{\partial y} + \frac{\partial W}{\partial z}). \tag{3}$$

In the ABL the 3-dimensional divergence $\nabla \cdot \vec{V} = \frac{\partial U}{\partial x} + \frac{\partial V}{\partial y} + \frac{\partial W}{\partial z}$ and the derivatives with respect to the horizontal directions can usually be neglected if the underlying surface is sufficiently homogeneous. Under these conditions ADV simplifies to

$$ADV = \frac{\partial UW}{\partial z}. \tag{4}$$

4. Reynolds averaging and the mean equation

The velocity components U and W in (3) are instantaneous values. To deal with the typical rapidly fluctuating velocity in turbulent flows Reynolds (1895) introduced a splitting of variables into a mean value and the deviation from the mean value. Ideally the mean value should be the ensamble mean. Applied to the atmosphere the latter

is obtained by averaging over a large number of realisations of each "weather event". This is of course not possible in practice. Instead a time average is used. The averaging period should be large enough to contain the turbulence, i.e. larger than the dominant time scale of the turbulence, but so short that it leaves the slovly varying "synoptic field" unsmoothed. As a compromise between these requirements an averaging period of 20 minutes is often used.

With Reynolds averaging any instantanous variable as for example U is written $U = \overline{U} + U^{'}$, where $\overline{U}$ is the time average of U over a certain period (~ 20 minutes) and $U^{'}$ the deviation from the mean value. By this procedure ADV can be written

$$ADV = \frac{\partial}{\partial z}(\overline{U} \cdot \overline{W} + \overline{U} \cdot W^{'} + \overline{W} \cdot U^{'} + U^{'}W^{'}). \tag{5}$$

The time average of ADV simply becomes

$$\overline{ADV} = \frac{\partial}{\partial z}(\overline{U} \cdot \overline{W} + \overline{U^{'}W^{'}}), \tag{6}$$

because by definition $\overline{\zeta^{'}} = 0$ and $\overline{\overline{\zeta}} = \overline{\zeta}$, where ζ can be any atmospheric variable. Furthermore, over flat terrain $\overline{W}$ is usually small in the ABL, so that the term $\frac{\partial}{\partial z}(\overline{U} \cdot \overline{W})$ can be neglected. With these approximations time averaging of equation (1) yields

$$\frac{\partial \overline{U}}{\partial t} + \frac{\partial}{\partial z}\overline{U^{'}W^{'}} = -\frac{1}{\overline{\rho}}\frac{\partial \overline{p}}{\partial x} + f\overline{V} + \frac{\partial}{\partial z}(\nu_M \frac{\partial \overline{U}}{\partial z}). \tag{7}$$

Now the forces on the rhs have been explicitely written. From left to right they are respectively the horizontal pressure gradient force, the Coriolis force and the molecular frictional force (all per unit mass). Variable p is mean pressure, $\overline{\rho}$ is the average density. f is the Coriolis parameter and ν_M the molecular kinematic viscosity. The second term on the lhs acts as friction in the mean flow. This can be seen more clearly by moving it to the rhs of the equation. The equation then reads

$$\frac{\partial \overline{U}}{\partial t} = -\frac{1}{\overline{\rho}}\frac{\partial \overline{p}}{\partial x} + f\overline{V} + \frac{\partial}{\partial z}(\nu_M \frac{\partial \overline{U}}{\partial z} - \overline{U^{'}W^{'}}). \tag{8}$$

The term $-\overline{U^{'}W^{'}}$ is the vertical momentum flux due to the rapid fluctuating part of the flow field. These rapid motions is a manifestation of turbulence. The momentum flux $-\overline{U^{'}W^{'}}$ is often called shear stress or Reynolds stress associated with mean motion in the x-direction. There are also contributions to the shear stress in this direction from $-\overline{U^{'}U^{'}}$ and $-\overline{U^{'}V^{'}}$, but they are usually small compared with $-\overline{U^{'}W^{'}}$, and were neglected in the derivation of (7).

The Reynolds stress is not measured regularly in a global network like for example temperature, wind velocity and surface pressure, and in numerical weather prediction models it is usually not a prognostic variable. Instead the Reynolds stress is parameterized in terms of "known" variables. The parameterization frequently applied makes use of an analogy to molecular friction, i.e.

$$-\overline{U^{'}W^{'}} = \nu_T \frac{\partial \overline{U}}{\partial z}. \tag{9}$$

Hence equation (8) can be written

$$\frac{\partial \overline{U}}{\partial t} = -\frac{1}{\overline{\rho}}\frac{\partial \overline{p}}{\partial x} + f\overline{V} + \frac{\partial}{\partial z}((\nu_M + \nu_T)\frac{\partial \overline{U}}{\partial z}). \tag{10}$$

From (10) it is clear that turbulence gives rise to friction in the mean flow in a way similar to molecular friction. For this reason ν_T is often called the eddy viscosity. However, it must be emphasized that ν_T behaves very differently from its molecular counterpart ν_M. The latter can be regarded as constant for the air ($\sim 1.5 \cdot 10^{-5} m^2 s^{-1}$), while ν_T is highly variable in space and time. Almost all the complexity associated with $-\overline{U'W'}$ is "hidden" in ν_T. The eddy viscosity is clearly a property of the flow, because its value varies with changing flow conditions. In contrast ν_M is independent of the air motions, i.e. a property of the air. Furthermore, ν_T is larger than ν_M by a factor of 10^4 to 10^5 in most of the ABL. Only in a mm-thin layer at the surface is ν_M larger than ν_T. This layer is called the viscous or laminar sublayer.

5. Physical interpretation of Reynolds stress and turbulent friction

The Reynolds stress $-\overline{U'W'}$ and the turbulent friction $\frac{\partial}{\partial z}(-\overline{U'W'})$ can be interpreted physically by considering a mean wind $\overline{U}$ increasing with height above a horizontal and homogeneous surface, and by considering turbulence as consisting of a continuum of eddies ranging from the mm-scale to the km-scale. The eddies are 3-dimensional filaments of air, generally with a component of rotation along all 3 space directions. In the interpretation of $-\overline{U'W'}$ it is only necessary to consider eddy motions in the vertical x-z plane.

Figure 3 shows a large and small eddy embedded in a mean flow increasing with height. At point 1 in the figure larger momentum is transported downward by eddy motion. Measurements of instantanous values of U and W at point 1 therefore are likely to show $U' > 0$ and $W' < 0$. In the same way, at point 2 lower momentum transported upward is likly to give $U' < 0$ and $W' > 0$. It is also clear that the same arguments apply for the smaller eddy at point 3 and 4. When averaged over a period of time we therefore get $\overline{U'W'} < 0$. This result shows that there is a downward transport of "eddy" momentum due to turbulence. If, at a given level, the downward transport of momentum from above is less than the downward transport to the layer below, there is a sink of momentum at the considered level. If we only consider the effect on the mean flow from the turbulence it follows from (8) that $\partial\overline{U}/\partial t < 0$. This explains why $\partial/\partial z(-\overline{U'W'})$ is called turbulent friction.

Basically, the origin of turbulence in a neutral stratified atmosphere is the velocity shear. If the velocity in Figure 3 was constant with height and the stratification was neutral there would be no turbulence in the flow. In the free atmosphere, i.e. above the ABL, this would also be the case if the wind shear was sufficiently weak. However, if the wind shear becomes sufficiently strong the flow becomes turbulent and it can be shown that the production of turbulent kinetic energy (TKE) then is $-\overline{U'W'} \cdot \partial\overline{U}/\partial z$. This term is called mechanical or shear production (S) of TKE.

Complexity is added, if there are layers in the atmosphere with stable or unstable stratification. The free atmosphere is usually stably stratified, but the ABL has a stratification that varies with latitude, position (land/sea), season and time of day. In

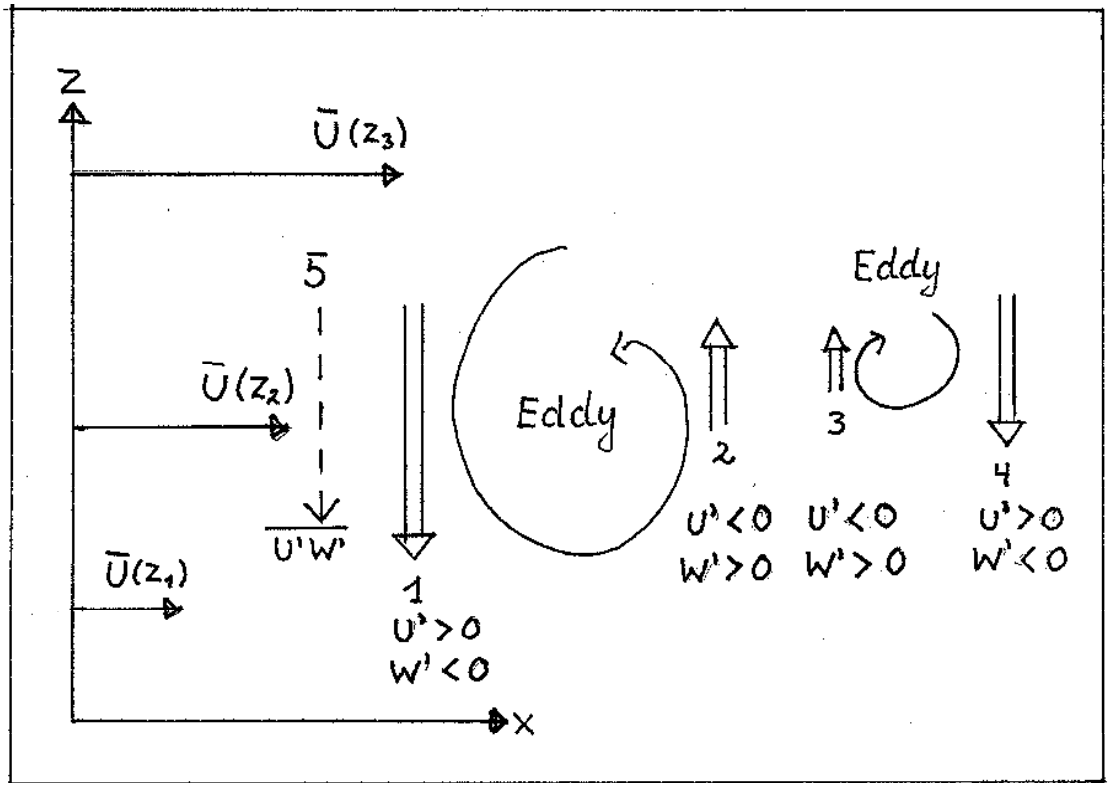

Figure 3: Turbulent momentum transport ($-\overline{U'W'}$) by eddies in the x-z plane of the ABL. See text for more explanation.

cloud free air the typical picture over land is that the ABL is unstably stratified at day and stably stratified at night. It will be demonstrated below that stratification has a very strong influence on the turbulence.

6. Turbulent heat flux

A potential temperature equation similar to that for momentum (1) can be derived from the first law of thermodynamics. It takes the form (per unit mass)

$$\frac{\partial\theta}{\partial t} + U\frac{\partial\theta}{\partial x} + V\frac{\partial\theta}{\partial y} + W\frac{\partial\theta}{\partial z} = \frac{1}{c_p\overline{\rho}}(\frac{p_0}{p})^{R/c_p}\Sigma D_i. \tag{11}$$

Here θ is the potential temperature, c_p is the heat capacity of air at constant pressure, p_0=1000 hPa is a reference pressure and ΣD_i is the sum of diabatic heating/cooling terms. Divergence of long and short wave radiation and of molecular heat flux as well as heating due to condensation and cooling due to evaporation may contribute to the rhs of (11). Usually the turbulent heat flux is much larger in the vertical than in the horizontal directions, in particular if the surface is homogeneous. Then (11) can be simplified to

$$\frac{\partial\theta}{\partial t} + W\frac{\partial\theta}{\partial z} = \frac{1}{c_p\overline{\rho}}(\frac{p_0}{p})^{R/c_p}\Sigma D_i. \tag{12}$$

Here our aim are to show the difference between the molecular and turbulent heating. The molecular heat flux in the vertical direction can be written as $H_m = -k_T\partial T/\partial z$, where k_T is the thermal conductivity of air. The molecular heating/cooling term in (12) is therefore

$$D_m = \frac{\partial}{\partial z}(k_T\frac{\partial T}{\partial z}), \tag{13}$$

i.e. with a form similar to the molecular friction in (8). In the ABL k_T can be regarded as constant, hence $D_m = k_T \partial^2 T/\partial z^2$. In text books about boundary layer meteorology the molecular heating/cooling term is often written as $k_T \partial^2 \theta/\partial z^2$. Apparently, this is different from the rhs of (12). However, it can be shown (by using Poisson's equation and the hydrostatic equation) that

$$\frac{\partial^2 \theta}{\partial z^2} = \frac{g}{c_p}\frac{1}{T}\frac{\partial \theta}{\partial z} + (\frac{p_0}{p})^{R/c_p}\frac{\partial^2 T}{\partial z^2} \tag{14}$$

In the ABL the first term on the rhs of (14) is between 1 and 2 orders of magnitude smaller than the second rhs term. Hence (14) can be approximated by

$$\frac{\partial^2 \theta}{\partial z^2} \equiv \frac{\partial^2}{\partial z^2}[(\frac{p_0}{p})^{R/c_p} T] \approx (\frac{p_0}{p})^{R/c_p}\frac{\partial^2 T}{\partial z^2}. \tag{15}$$

Stated in another way, it is permissible in the ABL to treat $(p_0/p)^{R/c_p}$ as a constant in (14). Then, if we only consider molecular heating/cooling (12) can be written

$$\frac{\partial \theta}{\partial t} + W\frac{\partial \theta}{\partial z} = \kappa_T \frac{\partial^2 \theta}{\partial z^2}, \tag{16}$$

where $\kappa_T = k_T/(\overline{\rho} c_p)$ is the thermal diffusivity. Reynolds averaging of (16) gives

$$\frac{\partial \overline{\theta}}{\partial t} = \frac{\partial}{\partial z}(\kappa_T \frac{\partial \overline{\theta}}{\partial z} - \overline{W'\theta'}) \tag{17}$$

Like for momentum the Reynolds term $-\overline{W'\theta'}$ (the kinematic turbulent heat flux in the vertical) is often parameterized by

$$-\overline{W'\theta'} = K_T \frac{\partial \overline{\theta}}{\partial z}, \tag{18}$$

where K_T is the thermal eddy diffusivity similar to its molecular counterpart κ_T. K_T is like ν_T for momentum a property of the fluid, while κ_T is a property of the air. Much of the complexity is hidden in K_T. The latter is usually several orders of magnitude larger than κ_T, which means that the effect on the mean potential temperature of the vertical heat flux to a good approximation is given by

$$\frac{\partial \overline{\theta}}{\partial t} = \frac{\partial}{\partial z}(K_T \frac{\partial \overline{\theta}}{\partial z}) \tag{19}$$

The behaviour of turbulence is very different in stable and unstable stratification.

7. Stable stratification

Here the mean potential temperature $\overline{\theta}$ increases with height (i.e. $\partial \overline{\theta}/\partial z > 0$) as shown in Figure 4. At point 1 in this figure air with higher $\overline{\theta}$ is transported downward by eddy motion. Measurement of instantanous values of θ and W are therefore likely to show $W' < 0$ and $\theta' > 0$. Likewise, at point 2 measurements are likely to show $W' > 0$ and $\theta' < 0$, because at this point air with lower $\overline{\theta}$ is transported upward by eddy

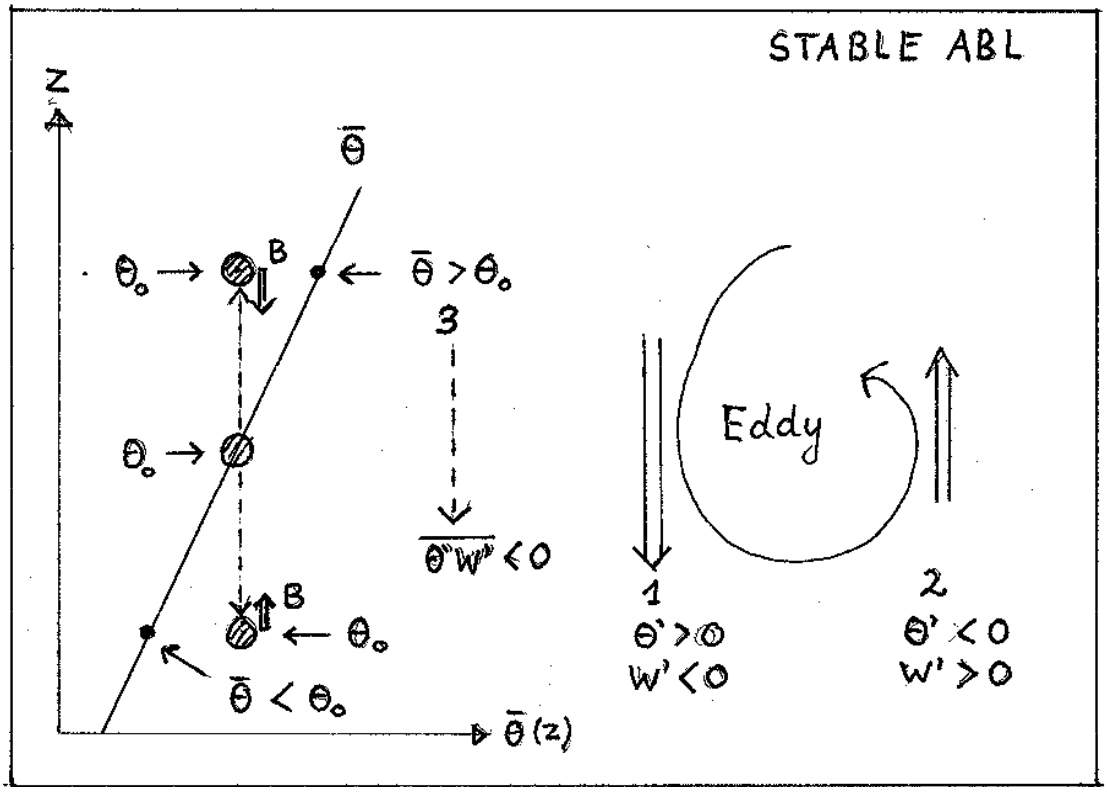

Figure 4: Vertical kinematic turbulent heat flux ($-\overline{W'\theta'}$) in the stably stratified ABL. $\overline{\theta}$ is the mean potential temperature profile, θ_0 the potential temperature of the air particle moved adiabatically up and down from its equilibrium position ($\theta_0 = \overline{\theta}$) and B the buoyancy force acting on the displaced particle. See text for further explanation.

motion. Averaged over a period of time we therefore must have $\overline{W'\theta'} < 0$, i.e. that there is a downward transport of heat by turbulence (a downward turbulent heat flux). If at a given level the turbulent heat flux from above is larger than the corresponding downward flux to the layer below, heat is stored and $\overline{\theta}$ increases with time ($\partial\overline{\theta}/\partial t > 0$) at the considered level. This happens if $\partial/\partial z(-\overline{W'\theta'}) > 0$ or with the parameterization in (18) if $\partial/\partial z(K_T \partial\overline{\theta}/\partial z) > 0$. Similarly there is a heat sink ($\partial\overline{\theta}/\partial t < 0$) if the downward heat flux from above is less than the downward heat flux to the layer below.

The rule is therefore that if the turbulent heat flux increases (becomes less negative) with height the air is cooled, and if it decreases (becomes more negative) with height the air is warmed. The former situation usually characterises clear night ABL's over land.

Vertical turbulent motions are damped in a stably stratified ABL, as illustrated in the left part of Figure 4. An air particle with potential temperature θ_0 pushed upward adiabatically from its equilibrium position will be colder than the surrounding air ($\theta_0 < \overline{\theta}$). The negative buoyancy force acting on the particle will eventually move it backward (downward) towards the equilibrium position. If the particle is pushed adiabatically downward from its equilibrium position it becomes warmer than the surrounding air ($\theta_0 > \overline{\theta}$), and positive buoyancy acting on the particle will soon move it backward (upward) towards the equilibrium position. The resistance against vertical motion in stable stratification occurs because turbulent motions on average move colder air upward and warmer air downward. In this process the potential energy of the air

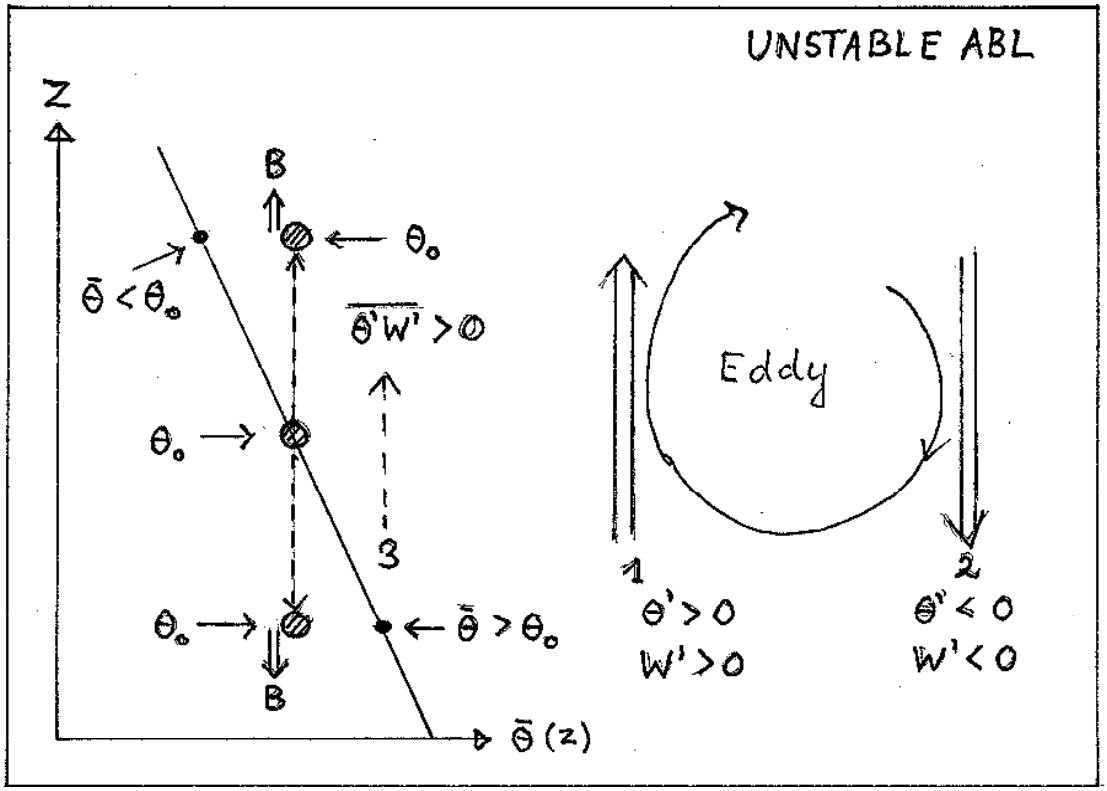

Figure 5: As Figure 4, but for the unstably stratified ABL.

increases, while the kinetic energy of the turbulent eddy motions decreases correspondingly. The turbulence weakens until it has reached an equilibrium between production and destruction of turbulent kinetic energy. The destruction of turbulence may become so strong that an equilibrium never is reached. In the latter case turbulence dies out completely.

7.1. Unstable stratification

Here $\overline{\theta}$ decreases with height ($\partial\overline{\theta}/\partial z < 0$) as shown in Figure 5. At point 1 in this figure air with higher $\overline{\theta}$ is transported upward by eddy motion. Measurements of instantanous values of of θ and W are therefore likely to show $\theta^{'} > 0$ and $W^{'} > 0$. Similarly, at point 2 measurements are likely to show $\theta^{'} < 0$ and $W^{'} < 0$, because at this point air with lower $\overline{\theta}$ is transported downward by eddy motion. Consequently we must have $\overline{W^{'}\theta^{'}} > 0$, i.e. the turbulent heat flux must be upward. Like for the stable case the air is cooled if the heat flux increases with height and it is warmed if the heat flux decreases with height. The latter situation characterises the ABL on clear days with sufficiently high insolation.

Vertical turbulent motions are enhanced in an unstably stratified ABL, as shown in the left part of Figure 5. An air particle with potential temperature θ_0 that is pushed upward adiabatically from its equilibrium level becomes warmer than the surrounding air ($\theta_0 > \overline{\theta}$), and the positive (upward) buoyancy force acting on the particle increases its upward motion. If the particle is pushed downward, it becomes colder than the surrounding air. Negative (downward) buoyancy will act on the particle and increase its downward motion. Air particles pushed away from their equilibrium positions by turbulence will be accelerated, resulting in more vigorous eddy motions. The on average

rising warmer air and sinking colder air in the unstable (convective) ABL decreases the potential energy of the air and increases the kinetic energy of the turbulent eddies correspondingly.

The potential temperature at the tropopause is usually much higher than the potential temperature at the surface. Therefore, as a rule the free atmosphere above the convective ABL is stably stratified. Frequently there is a "lid" of very stably stratified air on top of the convective ABL. In this layer, called the entrainment zone, turbulence penetrating from below dies out rapidly with height. See the typical $\overline{\theta}$-profile in the CBL in Figure 6. .

Turbulence in the convective ABL is often so vigorous that most of the ABL becomes well-mixed, i.e. with almost uniform (constant with height) mean profiles of atmospheric variables. For the potential temperature this means that the heating must be approximately uniform with height ($\partial/\partial z(\partial\overline{\theta}/\partial t) \approx 0$). According to (18) and (19) this implies a linear decrease with height of the kinematic turbulent heat flux $\overline{W'\theta'}$.

8. The turbulent kinetic energy budget

From the discussion of Figure 4 and 5 it is clear that buoyancy forces destroy turbulent kinetic energy (TKE) in case of stable stratification and generate TKE in case of unstable stratificatione. The TKE is the kinetic energy of the wind fluctuations, i.e.

$$TKE = \frac{1}{2}(\overline{u'^2 + v'^2 + w'^2}) \tag{20}$$

It can be shown that the buoyancy production/destruction term is given by $B = g/\overline{\theta} \cdot \overline{W'\theta'}$.

The TKE-equation can be written in symbolic (and approximated) form as

$$\frac{D(TKE)}{Dt} = S + B - D + T. \tag{21}$$

The equation is an approximation, because a pressure-velocity correlation term has been omitted. This term tends to spread a change in magnitude of fluctuations in one velocity component to the other two. The more complete TKE-equation is presented in for example Garratt, 1992. In (21) the shear production S and the buyancy production/destruction B has already been discussed. The remaining two terms are the molecular dissipation of TKE (term D) and the transport or redistribution of TKE within the ABL (term T). The dissipation D is always positive (or zero in case of no turbulence). In the surface layer (roughly the bottom one tenths of the ABL) and in the stably stratified ABL this also holds for the shear production S. The byouancy term B as well as the transport term T can be both sink and source terms for TKE. The latter is only a sink/source term locally. When integrated over the depth of the ABL it is zero. The buoyancy term must therefore be responsible for the observed significant difference between the stably and unstably stratified ABL.

In the convective ABL (CBL) the largest eddies have a vertical scale comparable with the depth of the CBL, but in the stably stratified ABL (SBL) the resistance against vertical motion limits the vertical scale of the largest eddies to a small fraction of the depth of the ABL. Consequently, the mixing by turbulence is much more local in the SBL, which means that significant vertical gradients of atmospheric variables can persist in the SBL. At high static stability the latter variables vary approximately linearly with height in the surface layer of the SBL.

In contrast, the mixing in the CBL is strong and nonlocal, which means that gradients of atmospheric variables are erased in the CBL, except near its top and bottom, where eddy motions are surpressed in the entrainment zone (the stable layer at the top of the CBL) and by the rigid surface, respectively. If we for example consider the mean wind speed profile $\overline{M}$ (Figure 7), it has a nearly constant value in the well-mixed part of the CBL and sharp gradients in the entrainment zone and in the surface layer. Through these layers the mixed layer value of $\overline{M}$ has to match the wind in the free atmosphere and $\overline{M} = 0$ at the surface, respectively.

9. The near-surface wind speed

On cloud free days with sufficient insolation it is often observed that the near-surface wind speed increases after sunrise and in the evening returns to the level before sunrise. This pattern can also be seen in climatological wind data, as shown in Figure 8. This figure shows the diurnal variation of a 10-year averaged (1958-67) wind speed for April at different heights along the Risø tower near Roskilde, Denmark. From sunrise to about 10 local time (LT) the wind speed decreases at the 123 m height and increases at the 7 m height, indicating that momentum is beeing mixed down from the upper level by turbulent eddies that are groving after sunrise as a result of the change in buoyancy from a negative to a positive value. After about 10 LT and until a few hours before sunset the wind speed varies in phase at the two levels. This does not mean that the mixing of momentum has ceased. Instead it indicates that the CBL after 10 LT has grown far beyond the 123 m level. Momentum from above is in this period mixed down to both the 123 and the 7 m level. From about 18 LT the wind speed remains almost constant (at the before-sunrise level) at the 123 m height, while it decreases at lower levels. This indicates that a SBL has formed at the bottom of the (former) CBL. Relatively strong turbulent friction initially in the newly formed SBL leads to a rapid decrease with time of the wind speed in the SBL. As the SBL becomes older the decrease in wind speed levels off, indicating a corresponding decrease in turbulent friction. Note also in Figure 8 how the gradient of mean wind speed is spread out over the whole layer below 123 m at night, while it is concentrated near the surface at day.

10. The nocturnal jet

The gradient Richardson number Ri, defined as

$$Ri = \frac{g}{\overline{\theta}} \frac{\frac{\partial \overline{\theta}}{\partial z}}{|\frac{\partial \vec{V}}{\partial z}|^2}, \tag{22}$$

is often used as a measure of stability. For convenience the averaging symbol has been omitted on the wind vector. It follows from the definition in (22) that Ri is positive

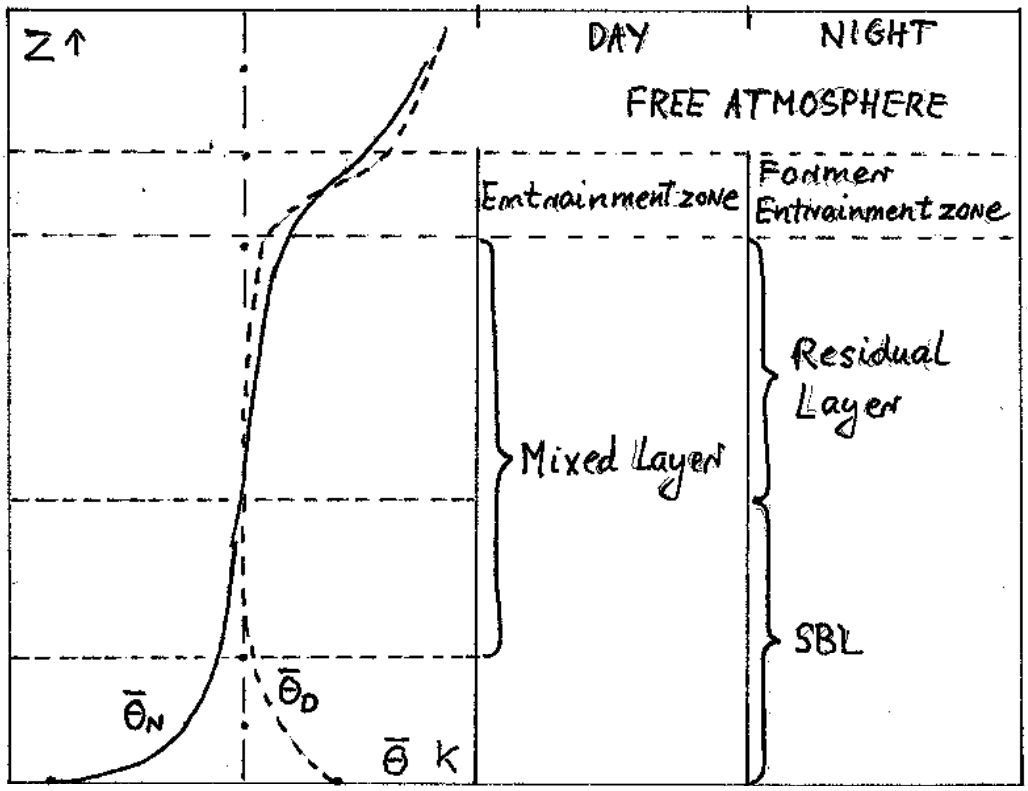

Figure 6: Schematic representation of the typical daytime ($\overline{\theta_D}$) and night time ($\overline{\theta_N}$) mean potential temperature profiles over land in the clear air ABL.

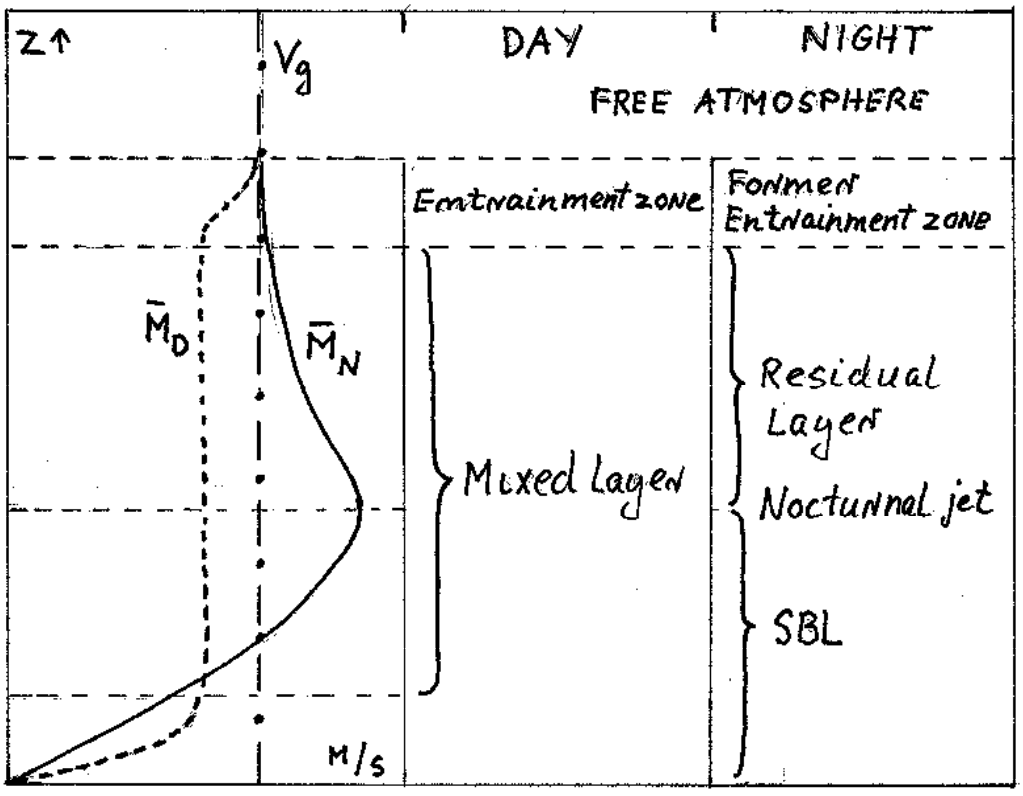

Figure 7: As Figure 6, but for the mean wind speed $\overline{M} = \left(\overline{U}^2 + \overline{V}^2\right)^{1/2}$. Note the nocturnal jet in the $\overline{M}_N$ profile near the top of the SBL.

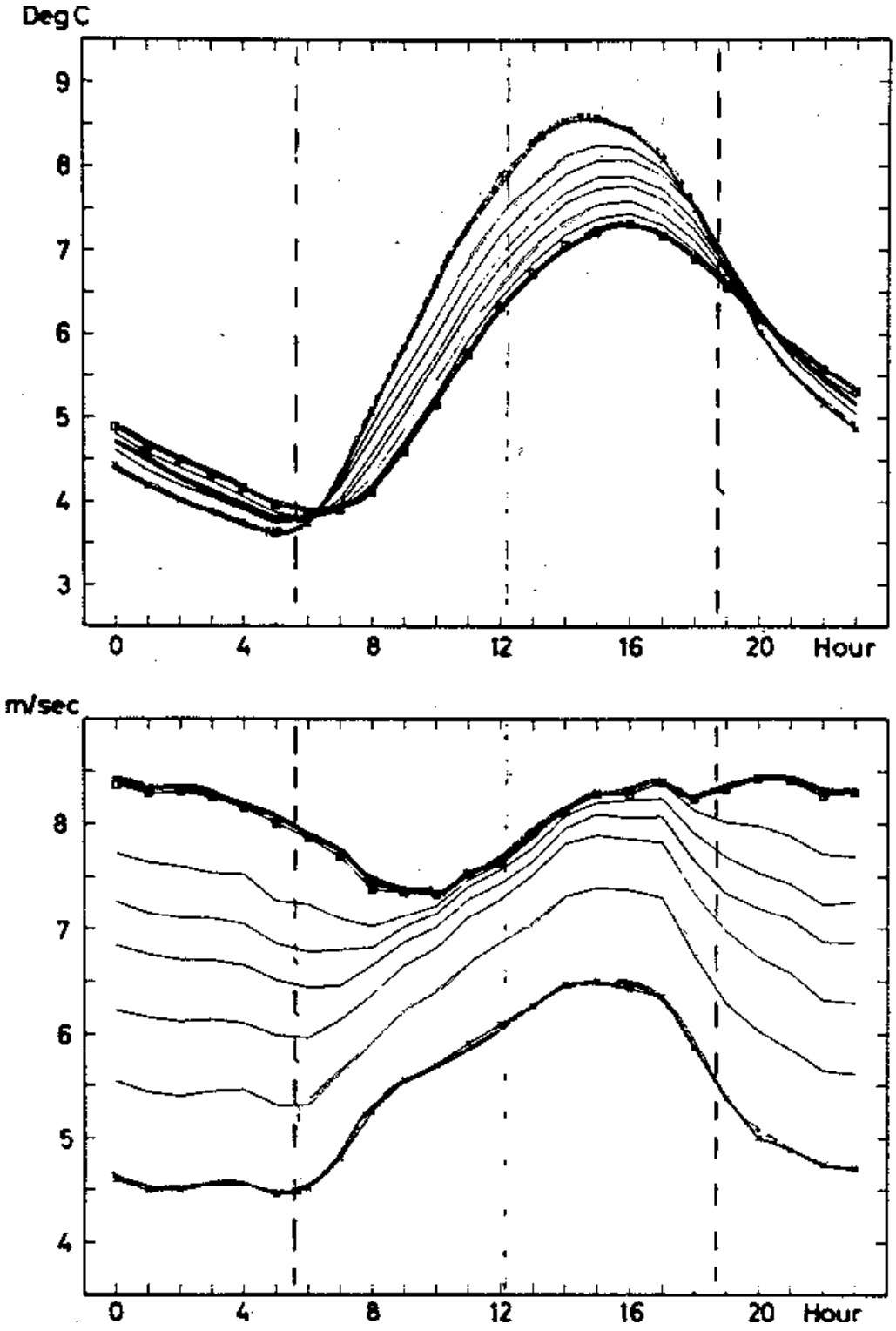

Figure 8: Climatological temperature and wind speed data from the Risø Tower near Roskilde, Denmark. Shown are 10 year averages (1958-67) values for April. Top: Temperature at heights 2, 7, 23, 39, 56, 72, 96 and 123 m, with thick lines for T_2 and T_{123}. Bottom: Wind speed at heights 7, 23, 39, 56, 72, 96 and 123 m, with thick lines for V_7 and V_{123} (from Petersen, 1975).

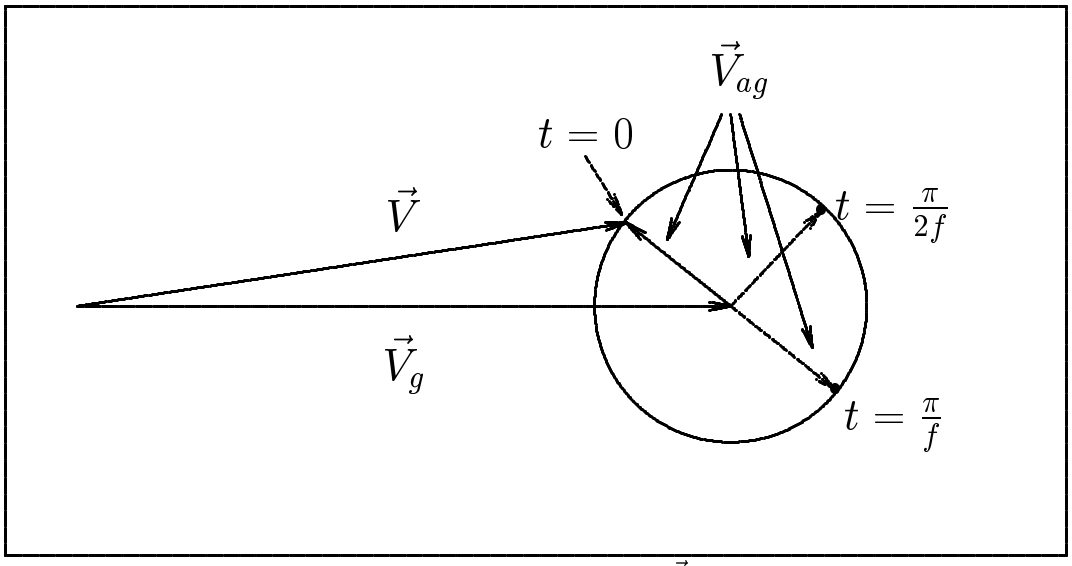

Figure 9: Initial oscillation of the ageostrophic wind ($\vec{V}_{ag}$) in the residual layer near the top of the SBL. Time $t = 0$ corresponds to near sunset. $\vec{V}_{ag}$ rotates clockwise around the arrowhead of the geostrophic wind $\vec{V}_g$. Between $t = \pi/2f$ and $t = \pi/f$, $|\vec{V}|$ attains its maximum value ($V_g + V_{ag}$).

and negative in the stably and unstably stratified ABL, respectively. Turbulence dies out if Ri becomes larger than a critical value $Ri_c \approx 0.25$. In the well-mixed former CBL (the residual layer) vertical gradients of both wind and potential temperature are small, and most importantly, Ri is proportional to $|\partial\vec{V}/\partial z|^{-2}$, which is large in the residual layer. Hence small changes in $\partial\overline{\theta}/\partial z$ will lead to large changes in Ri. Near sunset there is often radiative flux divergence at the top of the developing SBL. The latter results in an increase with time of $\partial\overline{\theta}/\partial z$ and Ri, for the latter to a value larger than Ri_c. This leads to a collapse of the turbulent frictional force and hence to a force imbalance in the residual layer. The force imbalance, involving the horizontal pressure gradient force and the Coriolis force gives rise to an initial oscillation of the ageostrophic wind $\vec{V}_{ag} = \vec{V} - \vec{V}_g$ in the residual layer with an initial period $2\pi/|f|$, where f is the Coriolis parameter. The initial oscillation of the ageostrophic wind (in case of a constant $\vec{V}_g$) is shown in Figure 9. According to this figure the wind attains its maximum ($\overline{V}_{max} = \overline{V}_g + \overline{V}_{ag}$) between $\pi/2|f|$ and $\pi/|f|$ hours (counted from sunset). The supergeostrophic wind blowing near the top of the SBL is called the nocturnal jet. The strength of this jet clearly depends on the magnitude of the ageostrophic wind in the residual layer at sunset. At 56°N we have $\pi/2|f| = 3.6$ hours, i.e. the nocturnal jet at this latitude has its maximum about 6 hours after sunset. In Figure 8 the nocturnal jet would therefore be expected to be at its maximum intensity around 01 LT with the jet core well above the 123 m level.

11. Land and sea ABL's

The structure of the cloud free ABL is often very different over land and adjacent seas. This is illustrated schematically in Figure 10. The overall (bulk) static stability in the ABL is mainly determined by advective and diabatic processes at the surface and top of the ABL. At the top of the ABL it is primarily advection proccesses that are

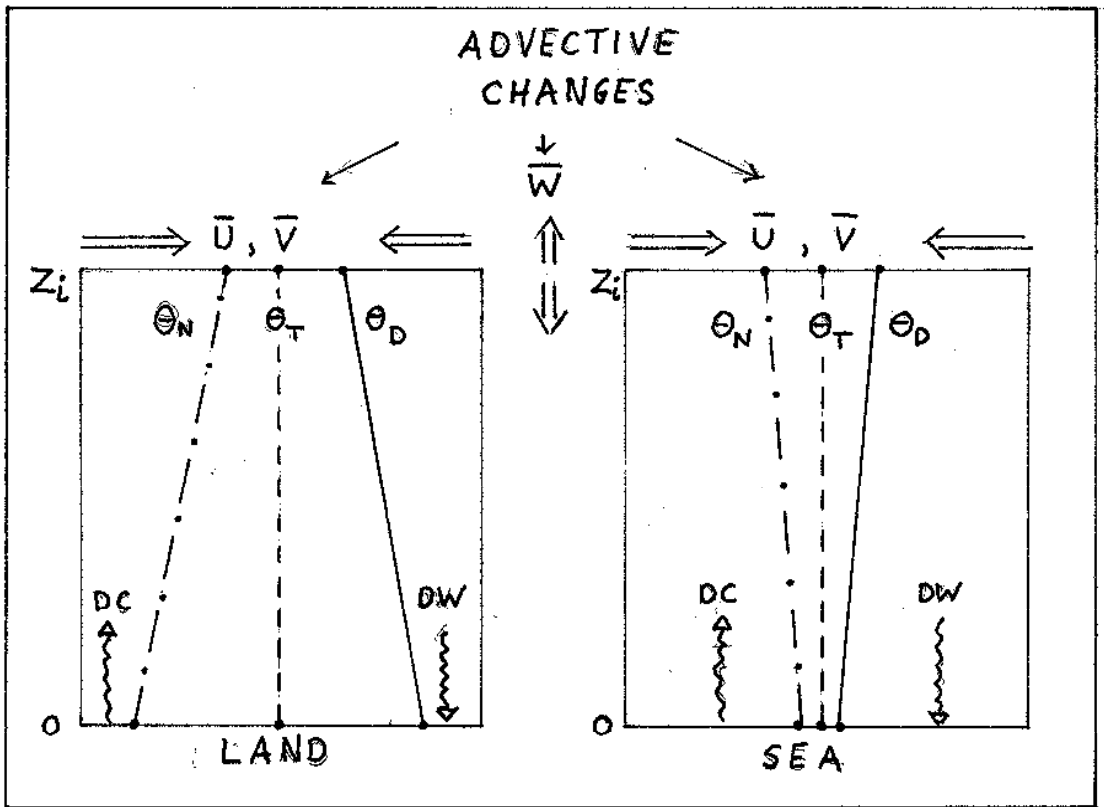

Figure 10: Schematic picture of the typical diurnal variation of the bulk static stability of the ABL over land and adjacent sea on days with land-sea breeze circulation. The daytime (θ_D) and the nighttime (θ_N) profiles show the out of phase variation over land and sea. θ_T is a neutral transition profile. Over land diabatic cooling (DC) and warming (DW) at the surface dominates over advection at the top (z_i) of the ABL. Over adjacent sea advection at the top (and in) the ABL dominates over DC and DW at the sea surface

responsible for changes in momentum, moisture and potential temperature. Over land, and in periods with high insolation the diurnal amplitude of the surface temperature is large, in particular if the surface is dry and without widespread vegetation. In contrast, the diurnal variation of the sea surface temperature is small. This is due to the large heat capacity of water and the turbulent mixing in the top layer of the sea. The typical situation is therefore that the diurnal variation in the bulk static stability in the ABL over land tends to be controlled by diabatic and turbulent processes at the surface. The corresponding diurnal amplitude over the sea tends instead to be controlled by advective processes at the top (and in) the ABL. Note that advection includes sinking and rising motion and the associated adiabatic warming and cooling, respectively.

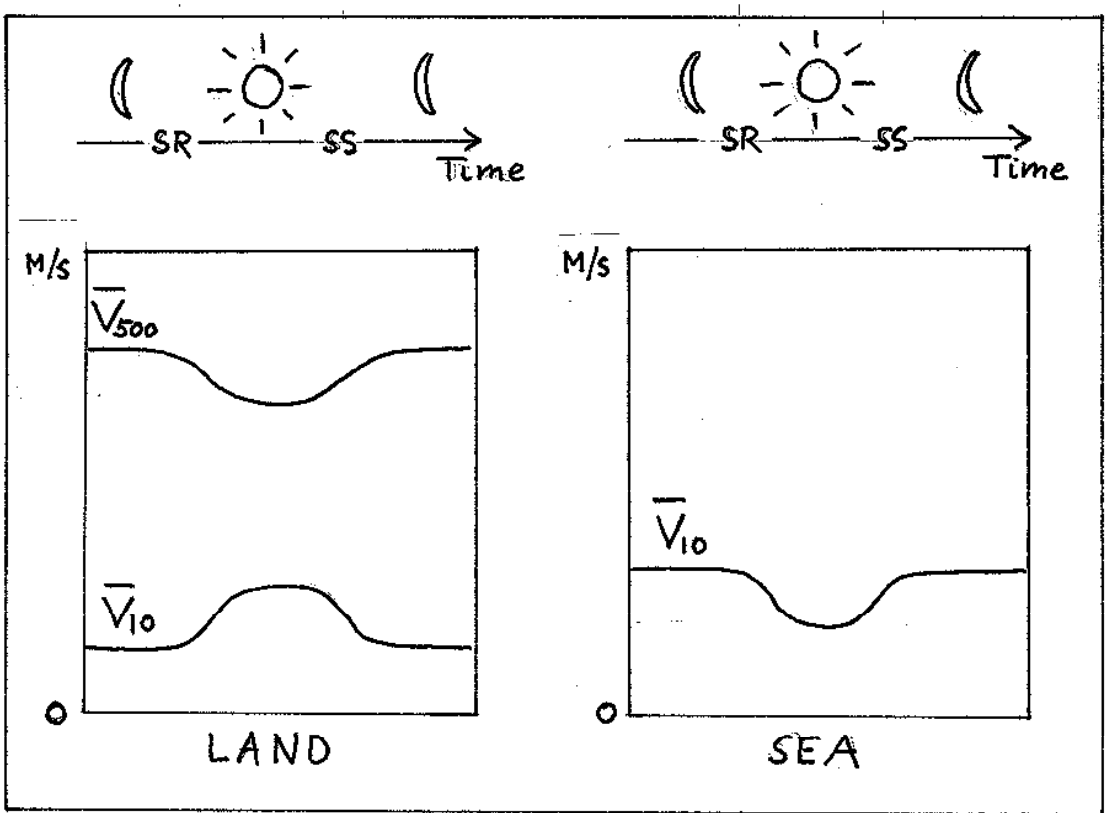

Figure 11: Schematics of the diurnal variation of the wind speed at 10 m height (V_{10} over land and adjacent sea on days with land-sea breeze circulation. A time axis is shown at the top of the figure with marks for sunrise (SR) and sunset (SS). Over land the wind speed at 500 m height is also indicated.

On days with a land-sea breeze circulation it is typical that the bulk static stability varies out of phase over land and adjacent sea. In daytime the radiative heating develops a CBL over land. The advection of relatively warm air from land to sea in the upper branch of the sea-breeze circulation leads to generation of a SBL over the sea. At nighttime radiative cooling at the surface creates a SBL over land, and the advection of relativly cold air from land to sea by the land-breeze circulation establishes a weak CBL over the sea. Due to the very different mixing properties in the SBL and CBL, as discussed in section 9, measurements of the wind speed at 10 m height over land and sea will typically be as shown schematically in Figure 11. In daytime an increase and a decrease in wind speed is observed over land and sea, respectively. At night the opposite happens. The tendency for out of phase variation of near-surface wind speed and direction is shown in Figure 12. This figure shows the diurnal variation of the anomaly in 10m-wind speed (Figure 12a), 10m-wind direction (Figure 12b), 2m-temperature (Figure 12c) and msl pressure (Figure 12d) at Anholt and Hesselø (two small islands in Cattegat) and Hvide Sande and Rømø at the west coast of Jutland. The former observations represents conditions over water, the latter (in particular Rømø) represents conditions over land.

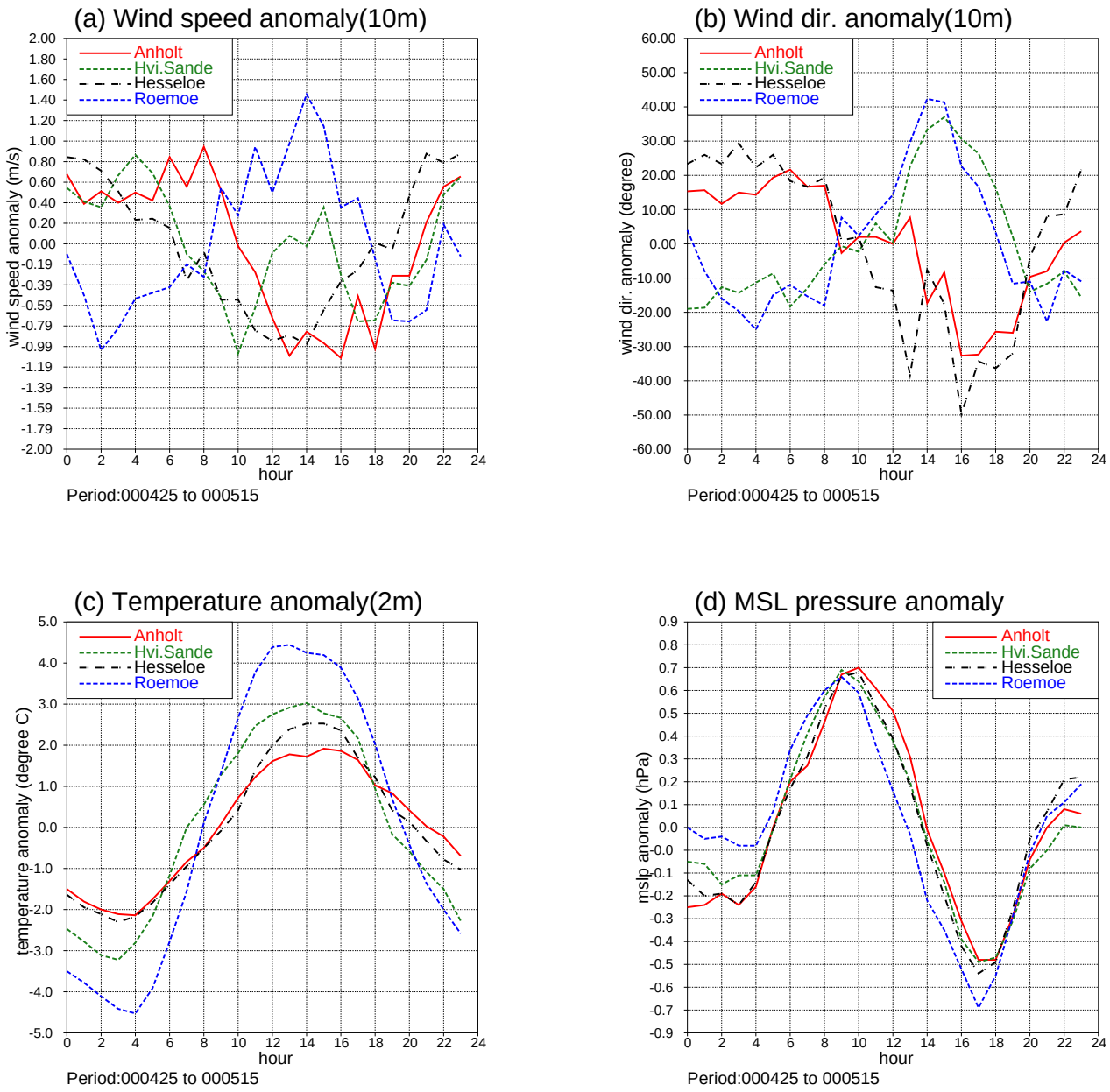

Figure 12: Observed diurnal variation of anomalies of (a): 10m-wind speed, (b): 10m-wind direction, (c): 2m-temperature and (d): mean sea level pressure at Anholt and Hesselø in Cattegat and at Hvide Sande and Rømø at the west coast of Jutland. Considered period is from 25 April to 15 May 2000. Time is in UTC. The prevailing wind in the period is from east-southeast. The observations from the west coast of Jutland therefore mainly show land conditions, which is in particular the case for Rømø. The influence of the upstream Ringkøbing Fjord can be seen in the data from Hvide Sande.

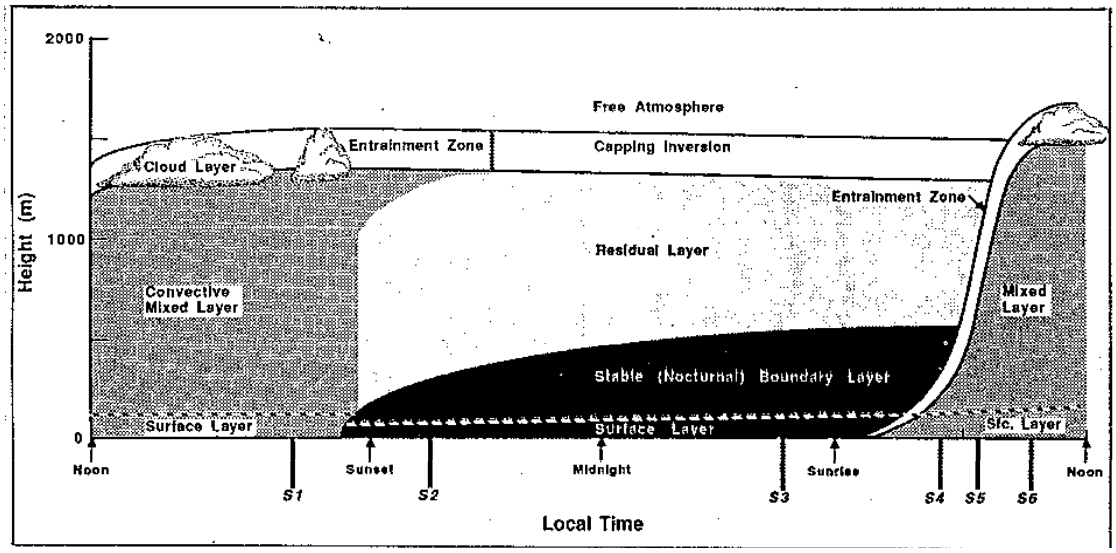

Figure 13: The ABL in heigh pressure regions over land consists of three major parts: a very turbulent mixed layer, a less-turbulent residual layer containing the former mixed-layer air, and a nocturnal SBL of sporadic turbulence. The mixed layer can be subdivided into a cloud layer and a subcloud layer. From Stull, 1988.

The period considered in Figure 12 is from 25 April to 15 May 2000. This period had prevailing east-southeasterly winds and almost unbroken clear sky conditions with a land-sea breeze circulation superposed on the mean flow.

12. Other aspects of the ABL

In this note the effect of water vapor on buoyancy in the unsaturated ABL has not been considered. However, this effect can be included simply by replacing $\overline{\theta}$ with the virtual potential temperature $\overline{\theta_v} = \overline{\theta}(1+\epsilon\overline{q})$, where $\epsilon = 0.61$ and $\overline{q}$ is the mean specific humidity.

Vertical profiles of mean specific humidity in the ABL have not been presented. They are quite similar to the $\overline{\theta}$ profiles, but it must be noted that $\partial\overline{q}/\partial z$ usually is weakly negative in the well-mixed part of the CBL. This is a consequence of the export of humidity from the CBL to the dry atmosphere above. In the upper part of the well-mixed layer $\partial\overline{\theta}/\partial z$ is weakly positive due to the downward turbulent transport of heat from the entrainment zone. It actually has the consequence that the turbulent heat flux is upward and $\partial\overline{\theta}/\partial z > 0$ in a part of the well-mixed layer, i.e. the turbulent heat flux is upgradient (from "cold" to "warm") in this region. In the latter region the parameterization in (18) breakes down and is often replaced by the "non-local" parameterization

$$-\overline{W'\theta'} = K_T(\frac{\partial\overline{\theta}}{\partial z} - \gamma_\theta), \tag{23}$$

where $\gamma_\theta > 0$ is a countergradient depending mainly on buoyancy. In terms of eddies one can think of the largest eddies as beeing responsible for the major part of the upgradient heat transport. These eddies do not care about the sign of $\partial\overline{\theta}/\partial z$ locally in the CBL. What counts is the sign of the potential temperature difference across the CBL.

As a summary of conditions over land we show in Figure 13 the typical diurnal variation in the ABL over land on days with significant insolation. The typical daytime and nighttime vertical profiles of potential temperature and wind speed were shown in Figures 6 and 7.

References

Ekman, V.W. (1905). On the influence of the Earth's rotation on the ocean currents. On the influence of the Earth's rotation on the ocean currents. *Arkiv. Mat. Astrom. Fysik*, **2**, 1–53.

Garratt, J.R. (1992). The atmospheric boundary layer. . *Cambridge University Press*, 316 pp.

Petersen, E.L. (1975). On the Kinetic Energy Spectrum of Atmospheric Motions in the Planetary Boundary Layer. *Risø Report no. 285*

Reynolds, O. (1895) On the dynamical theory of incompressible viscous fluids and the determination of the criterion.. *Phil. Trans. Roy. Soc. London***A186**, 123–64..

Stull, R.B. (1988) An Introduction to Boundary Layer Meteorology.. *Kluwer Academic Publishers*, 666 pp.

DANISH METEOROLOGICAL INSTITUTE

Scientific Reports

Scientific reports from the Danish Meteorological Institute cover a variety of geophysical fields, i.e. meteorology (including climatology), oceanography, subjects on air and sea pollution, geomagnetism, solar-terrestrial physics, and physics of the middle and upper atmosphere.

Reports in the series within the last five years:

No. 97-1
E. Friis Christensen og C. Skøtt: Contributions from the International Science Team. The Ørsted Mission - a pre-launch compendium

No. 97-2
Alix Rasmussen, Sissi Kiilsholm, Jens Havskov Sørensen, Ib Steen Mikkelsen: Analysis of tropospheric ozone measurements in Greenland: Contract No. EV5V-CT93-0318 (DG 12 DTEE): DMI's contribution to CEC Final Report Arctic Trophospheric Ozone Chemistry ARCTOC

No. 97-3
Peter Thejll: A search for effects of external events on terrestrial atmospheric pressure: cosmic rays

No. 97-4
Peter Thejll: A search for effects of external events on terrestrial atmospheric pressure: sector boundary crossings

No. 97-5
Knud Lassen: Twentieth century retreat of sea-ice in the Greenland Sea

No. 98-1
Niels Woetman Nielsen, Bjarne Amstrup, Jess U. Jørgensen:
HIRLAM 2.5 parallel tests at DMI: sensitivity to type of schemes for turbulence, moist processes and advection

No. 98-2
Per Høeg, Georg Bergeton Larsen, Hans-Henrik Benzon, Stig Syndergaard, Mette Dahl Mortensen: The GPSOS project
Algorithm functional design and analysis of ionosphere, stratosphere and troposphere observations

No. 98-3
Mette Dahl Mortensen, Per Høeg:
Satellite atmosphere profiling retrieval in a nonlinear troposphere
Previously entitled: Limitations induced by Multipath

No. 98-4
Mette Dahl Mortensen, Per Høeg:
Resolution properties in atmospheric profiling with GPS

No. 98-5
R.S. Gill and M. K. Rosengren
Evaluation of the Radarsat imagery for the operational mapping of sea ice around Greenland in 1997

No. 98-6
R.S. Gill, H.H. Valeur, P. Nielsen and K.Q. Hansen: Using ERS SAR images in the operational mapping of sea ice in the Greenland waters: final report for ESA-ESRIN's: pilot projekt no. PP2.PP2.DK2 and 2nd announcement of opportunity for the exploitation of ERS data projekt No. AO2..DK 102

No. 98-7
Per Høeg et al.: GPS Atmosphere profiling methods and error assessments

No. 98-8
H. Svensmark, N. Woetmann Nielsen and A.M. Sempreviva: Large scale soft and hard turbulent states of the atmosphere

No. 98-9
Philippe Lopez, Eigil Kaas and Annette Guldberg: The full particle-in-cell advection scheme in spherical geometry

No. 98-10
H. Svensmark: Influence of cosmic rays on earth's climate

No. 98-11
Peter Thejll and Henrik Svensmark: Notes on the method of normalized multivariate regression

No. 98-12
K. Lassen: Extent of sea ice in the Greenland Sea 1877-1997: an extension of DMI Scientific Report 97-5

No. 98-13
Niels Larsen, Alberto Adriani and Guido DiDonfrancesco: Microphysical analysis of polar stratospheric clouds observed by lidar at McMurdo, Antarctica

No.98-14
Mette Dahl Mortensen: The back-propagation method for inversion of radio occultation data

No. 98-15
Xiang-Yu Huang: Variational analysis using spatial filters

No. 99-1
Henrik Feddersen: Project on prediction of climate variations on seasonel to interannual timescales (PROVOST) EU contract ENVA4-CT95-0109: DMI contribution to the final report:Statistical analysis and post-processing of uncoupled PROVOST simulations

No. 99-2
Wilhelm May: A time-slice experiment with the ECHAM4 A-GCM at high resolution: the experimental design and the assessment of climate change as compared to a greenhouse gas experiment with ECHAM4/OPYC at low resolution

No. 99-3
Niels Larsen et al.: European stratospheric monitoring stations in the Artic II: CEC Environment and Climate Programme Contract ENV4-CT95-0136. DMI Contributions to the project

No. 99-4
Alexander Baklanov: Parameterisation of the deposition processes and radioactive decay: a review and some preliminary results with the DERMA model
No. 99-5
Mette Dahl Mortensen: Non-linear high resolution inversion of radio occultation data

No. 99-6
Stig Syndergaard: Retrieval analysis and methodologies in atmospheric limb sounding using the GNSS radio occultation technique

No. 99-7
Jun She, Jacob Woge Nielsen: Operational wave forecasts over the Baltic and North Sea

No. 99-8
Henrik Feddersen: Monthly temperature forecasts for Denmark - statistical or dynamical?

No. 99-9
P. Thejll, K. Lassen: Solar forcing of the Northern hemisphere air temperature: new data

No. 99-10
Torben Stockflet Jørgensen, Aksel Walløe Hansen: Comment on "Variation of cosmic ray flux and global coverage - a missing link in solar-climate relationships" by Henrik Svensmark and Eigil Friis-Christensen

No. 99-11
Mette Dahl Meincke: Inversion methods for atmospheric profiling with GPS occultations

No. 99-12
Hans-Henrik Benzon; Laust Olsen; Per Høeg: Simulations of current density measurements with a Faraday Current Meter and a magnetometer

No. 00-01
Per Høeg; G. Leppelmeier: ACE - Atmosphere Climate Experiment

No. 00-02
Per Høeg: FACE-IT: Field-Aligned Current Experiment in the Ionosphere and Thermosphere

No. 00-03
Allan Gross: Surface ozone and tropospheric chemistry with applications to regional air quality modeling. PhD thesis

No. 00-04
Henrik Vedel: Conversion of WGS84 geometric heights to NWP model HIRLAM geopotential heights

No. 00-05
Jérôme Chenevez: Advection experiments with DMI-Hirlam-Tracer

No. 00-06
Niels Larsen: Polar stratospheric clouds micro-physical and optical models

No. 00-07
Alix Rasmussen: "Uncertainty of meteorological parameters from DMI-HIRLAM"

No. 00-08
A.L. Morozova: Solar activity and Earth's weather. Effect of the forced atmospheric transparency changes on the troposphere temperature profile studied with atmospheric models

No. 00-09
Niels Larsen, Bjørn M. Knudsen, Michael Gauss, Giovanni Pitari: Effects from high-speed civil traffic aircraft emissions on polar stratospheric clouds

No. 00-10
Søren Andersen: Evaluation of SSM/I sea ice algorithms for use in the SAF on ocean and sea ice, July 2000

No. 00-11
Claus Petersen, Niels Woetmann Nielsen: Diagnosis of visibility in DMI-HIRLAM

No. 00-12
Erik Buch: A monograph on the physical oceanography of the Greenland waters

No. 00-13
M. Steffensen: Stability indices as indicators of lightning and thunder

No. 00-14
Bjarne Amstrup, Kristian S. Mogensen, Xiang-Yu Huang: Use of GPS observations in an optimum interpolation based data assimilation system

No. 00-15
Mads Hvid Nielsen: Dynamisk beskrivelse og hydrografisk klassifikation af den jyske kyststrøm

No. 00-16
Kristian S. Mogensen, Jess U. Jørgensen, Bjarne Amstrup, Xiaohua Yang and Xiang-Yu Huang: Towards an operational implementation of HIRLAM 3D-VAR at DMI

No. 00-17
Sattler, Kai; Huang, Xiang-Yu: Structure function characteristics for 2 meter temperature and relative humidity in different horizontal resolutions

No. 00-18
Niels Larsen, Ib Steen Mikkelsen, Bjørn M. Knudsen m.fl.: In-situ analysis of aerosols and gases in the polar stratosphere. A contribution to THESEO. Environment and climate research programme. Contract no. ENV4-CT97-0523. Final report

No. 00-19
Amstrup, Bjarne: EUCOS observing system experiments with the DMI HIRLAM optimum interpolation analysis and forecasting system

No. 01-01
V.O. Papitashvili, L.I. Gromova, V.A. Popov and O. Rasmussen: Northern polar cap magnetic activity index PCN: Effective area, universal time, seasonal, and solar cycle variations

No. 01-02
M.E. Gorbunov: Radioholographic methods for processing radio occultation data in multipath regions

No. 01-03
Niels Woetmann Nielsen; Claus Petersen: Calculation of wind gusts in DMI-HIRLAM

No. 01-04
Vladimir Penenko; Alexander Baklanov: Methods of sensitivity theory and inverse modeling for estimation of source parameter and risk/vulnerability areas

No. 01-05
Sergej Zilitinkevich; Alexander Baklanov; Jutta Rost; Ann-Sofi Smedman, Vasiliy Lykosov and Pierluigi Calanca: Diagnostic and prognostic equations for the depth of the stably stratified Ekman boundary layer

No. 01-06
Bjarne Amstrup: Impact of ATOVS AMSU-A radiance data in the DMI-HIRLAM 3D-Var analysis and forecasting system

No. 01-07
Sergej Zilitinkevich; Alexander Baklanov: Calculation of the height of stable boundary layers in operational models

No. 01-08
Vibeke Huess: Sea level variations in the North Sea – from tide gauges, altimetry and modelling

No. 01-09
Alexander Baklanov and Alexander Mahura: Atmospheric transport pathways, vulnerability and possible accidental consequences from nuclear risk sites: methodology for probabilistic atmospheric studies

No. 02-01
Bent Hansen Sass and Claus Petersen: Short range atmospheric forecasts using a nudging procedure to combine analyses of cloud and precipitation with a numerical forecast model

No. 02-02
Erik Buch: Present oceanographic conditions in Greenland waters

No. 02-03
Bjørn M. Knudsen, Signe B. Andersen and Allan Gross: Contribution of the Danish Meteorological Institute to the final report of SAMMOA. CEC contract EVK2-1999-00315: Spring-to.-autumn measurements and modelling of ozone and active species

No. 02-04
Nicolai Kliem: Numerical ocean and sea ice modelling: the area around Cape Farewell (Ph.D. thesis)